

Global extreme wave height variability based on satellite data

Cristina Izaguirre,¹ Fernando J. Méndez,¹ Melisa Menéndez,¹ and Inigo J. Losada¹

Received 28 February 2011; revised 30 March 2011; accepted 31 March 2011; published 25 May 2011.

[1] The spatial and temporal variability of the extreme significant wave height (SWH) in the ocean is presented. The study has been performed using a highly reliable dataset from several satellite altimeter missions, which provide a good worldwide coverage for the period 1992 onwards. A non-stationary extreme value analysis, which models seasonality and interannual variations, has been applied to characterize the extreme SWH. The interannual variability is explained through variations in the atmosphere and ocean systems, represented by different climate indices, allowing a quantitative contribution of the climate-related patterns. Results demonstrate the strong relationship between the interannual variability of extreme SWH and different ocean and atmosphere variations. A contribution of the AO and NAO indices in the North Atlantic ocean (e.g., every positive unit of the AO explains up to 70 cm of extreme wave height south of Iceland), the NINO3 in the Pacific (every negative unit of NINO3 explains up to 60 cm of extreme wave height in the Drake Passage), the SAM in the Southern ocean and the DMI in the Indian ocean reveal these climate patterns as the most relevant in the interannual extreme wave climate.

Citation: Izaguirre, C., F. J. Méndez, M. Menéndez, and I. J. Losada (2011), Global extreme wave height variability based on satellite data, *Geophys. Res. Lett.*, 38, L10607, doi:10.1029/2011GL047302.

1. Introduction

[2] The extreme events of significant wave height are crucial in the development of different natural processes. However, most of the times, they have negative effects on coastal structures, maritime works, ships or coastal communities. A good knowledge of the spatial and temporal extreme wave climate variability can help us to better understand natural processes while at the same time prevent social and economic disasters.

[3] Interannual wave climate variability depends on large-scale changes in the atmosphere-ocean systems, which are often represented by the El Niño Southern Oscillation (ENSO) or other regional climate patterns around the world. For instance, *Gulev and Grigorieva* [2004] found that mean significant wave height (SWH) in the Pacific is correlated with ENSO, *Woolf and Challenor* [2002] related interannual wave height variability in the North Atlantic with the NAO pattern, and *Lionello and Sanna* [2005] correlated variations in the monthly average SWH in the Mediterranean Sea

with NAO and Indian Monsoon. Referring to extreme wave climate, although several studies have focused on the teleconnections between extreme wave height and climate processes [*Wang and Swail*, 2001; *Menéndez et al.*, 2008; *Izaguirre et al.*, 2010] there is still a need to improve the knowledge of how changes in remote or regional atmospheric circulation affect worldwide extreme wave climate variability.

[4] The goal of this work is to model and quantify the spatial and temporal variability of extreme wave climate around the world, focusing on seasonal and interannual variations of monthly maxima of SWH (H_s).

2. Data

[5] Buoys and satellite measurements are the most appropriate data sets to characterize wave climate. However, only altimeter data are able to provide a good homogeneous coverage to carry out a worldwide study. In this study, we have used six different satellite missions from the period between 1992–2010: TOPEX, Jason-1, Jason-2, Envisat, GFO and ERS-2 (<http://www.avisio.oceanobs.com/>). The calibration procedures summarized by *Cotton* [1998] and *Woolf and Challenor* [2002], and later updated by *Hemer et al.* [2010] using extra years and additional satellite missions have been applied to the SWH altimeter. To achieve a good spatial resolution in which enough satellite passes must be ensured, we have defined cells in a 3° longitude by 2° latitude grid (where we aggregate individual measurements along the satellite tracks, selecting the monthly maximum H_s , and checking the interdependency between consecutive months [*Méndez et al.*, 2007]). Cells with less than 10% of the maximum number of data per cell ($N_{\max} = 937425$) have been rejected.

3. Extreme Value Model

3.1. Time-Dependent GEV Approach

[6] The study of seasonal-to-interannual variability of significant wave height can be faced by fitting a standard regression model to the original time series. This is the appropriate procedure when working with mean values or given percentiles of wave height in a unit of time (month, year), but referring to extreme values, this approach is not valid since we need to analyze changes in the probability of high return period values.

[7] In this study, we propose a statistical model based on a time-dependent GEV distribution of the SWH monthly maxima values from each defined cell using a scale factor, $k(t)$, that corrects the inhomogeneity in the number of data through time due to the addition of different satellite missions [*Izaguirre et al.*, 2010] and the bias of monthly maxima from satellite, due to the sparse temporal sampling provided by

¹Environmental Hydraulics Institute, Universidad de Cantabria, Santander, Spain.

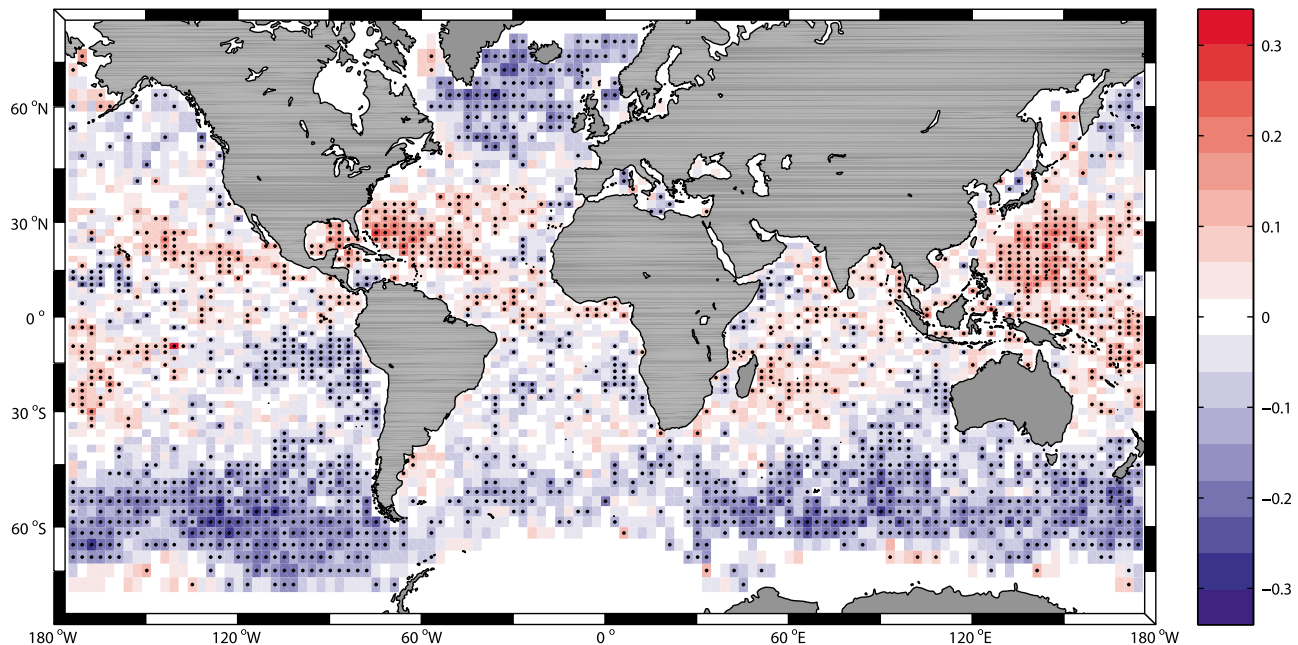


Figure 1. Spatial variability of the shape parameter of extreme wave height distribution around the world. Only statistically significant values at the 90% confidence interval are dotted.

the altimeter. The GEV cumulative distribution function is given by

$$F_t(z) = \begin{cases} \exp \left\{ -k(t) \left[1 + \xi^* \left(\frac{z - \mu^*(t)}{\psi^*(t)} \right) \right]_+^{-1/\xi^*} \right\} & \xi^* \neq 0 \\ \exp \left\{ -k(t) \exp \left[- \left(\frac{z - \mu^*(t)}{\psi^*(t)} \right) \right] \right\} & \xi^* = 0 \end{cases} \quad (1)$$

where $[a]_+ = \max[a, 0]$, $\mu(t)$ is the location parameter, $\psi(t)$ is the scale parameter and ξ is the shape parameter which informs us about the tail of the distribution ($\xi < 0$, $\xi = 0$, $\xi > 0$ for the Weibull, Gumbel and Fréchet families, respectively). The scale factor is defined as $k(t) = \alpha \cdot n(t)/N$ where $n(t)$ is the number of satellite observations in month t , $N = 720$ hours per month and α is a parameter to be estimated. We have obtained $\alpha = 0.6$ as the best estimate for this particular cell domain ($3^\circ \times 2^\circ$). This value of α has been obtained minimizing the root mean square error and the scatter index, comparing the satellite data and the buoy monthly maxima statistical distribution in several deep water (20) buoys around the world.

3.2. Modelling Variability

[8] Extreme wave climate at seasonal-to-interannual scales is considered by two models based on nested properties. We model seasonality using harmonic functions [Menéndez *et al.*, 2009], introducing the annual cycle in the location and scale parameters, $\mu(t) = \beta_0 + \beta_1 \cos(\omega t) + \beta_2 \sin(\omega t)$ and $\psi(t) = \alpha_0 + \alpha_1 \cos(\omega t) + \alpha_2 \sin(\omega t)$, where β_0 and α_0 are mean values, β_i and α_i are the amplitudes of the harmonics, $\omega = 2\pi \text{ year}^{-1}$ and t is given in years. A constant shape parameter, ξ , is included when significant at the 90% confidence interval (using the likelihood-ratio test).

[9] Regarding the interannual variability of wave climate, we assume it is affected by changes in the zonal circulation of the atmosphere [Izaguirre *et al.*, 2010] and by meridional

wind components. Wind sea, and swell may show different interannual variability due to different mechanism [Hogben, 1995]. Ten climate patterns have been used to investigate teleconnections in the worldwide extreme wave climate variations: the Arctic Oscillation (AO); the Southern Annular Mode (SAM); a descriptor of the El Niño–Southern Oscillation (NINO3); the Pacific North America Index (PNA); the North Atlantic Oscillation (NAO); the East Atlantic Pattern (EA); the East Atlantic–Western Russia pattern (EA/WR); the Scandinavian index (SCA); a descriptor of the Indian Ocean Dipole (the Dipole Mode Index, DMI); and the Quasi-Biennial Oscillation (QBO). SAM was selected from the British Antarctic Survey (<http://www.nerc-bas-ac-uk/icd/gjma>); DMI from the Japan Marine Science and Technology Center (<http://www.jamstec.go.jp>); NAO from the Climate Research Unit University of East Anglia (<http://www.cru.uea.ac.uk/cru>); and the rest of climate indices from the NOAA–National Weather Service (<http://www.cpc.ncep.noaa.gov>). All the indices are defined in a monthly scale. Once we have captured seasonality, the statistical relationship of a climate index is formulated as an additive covariate of the location parameter. For instance, for the NINO3: $\mu(t) = \beta_0 + \beta_1 \cos(\omega t) + \beta_2 \sin(\omega t) + \beta_{NINO3} NINO3(t)$, where β_{NINO3} indicates the sensitivity of the NINO3 in the extreme wave height ($^\circ\text{C}$ per unit of NINO3). Similar models are built for each climate index. Study of the interdecadal variability is not considered due to the relatively short length of the satellite records.

4. Results and Discussion

4.1. Seasonal Variability

[10] First, the seasonal model has been fitted to each $3^\circ \times 2^\circ$ cell of the global grid, testing the inclusion of the constant shape parameter (ξ_0) at a level of significance of 0.1. Figure 1 shows the spatial distribution of the shape parameter. Tropical areas where high cyclone and typhoon activity occur

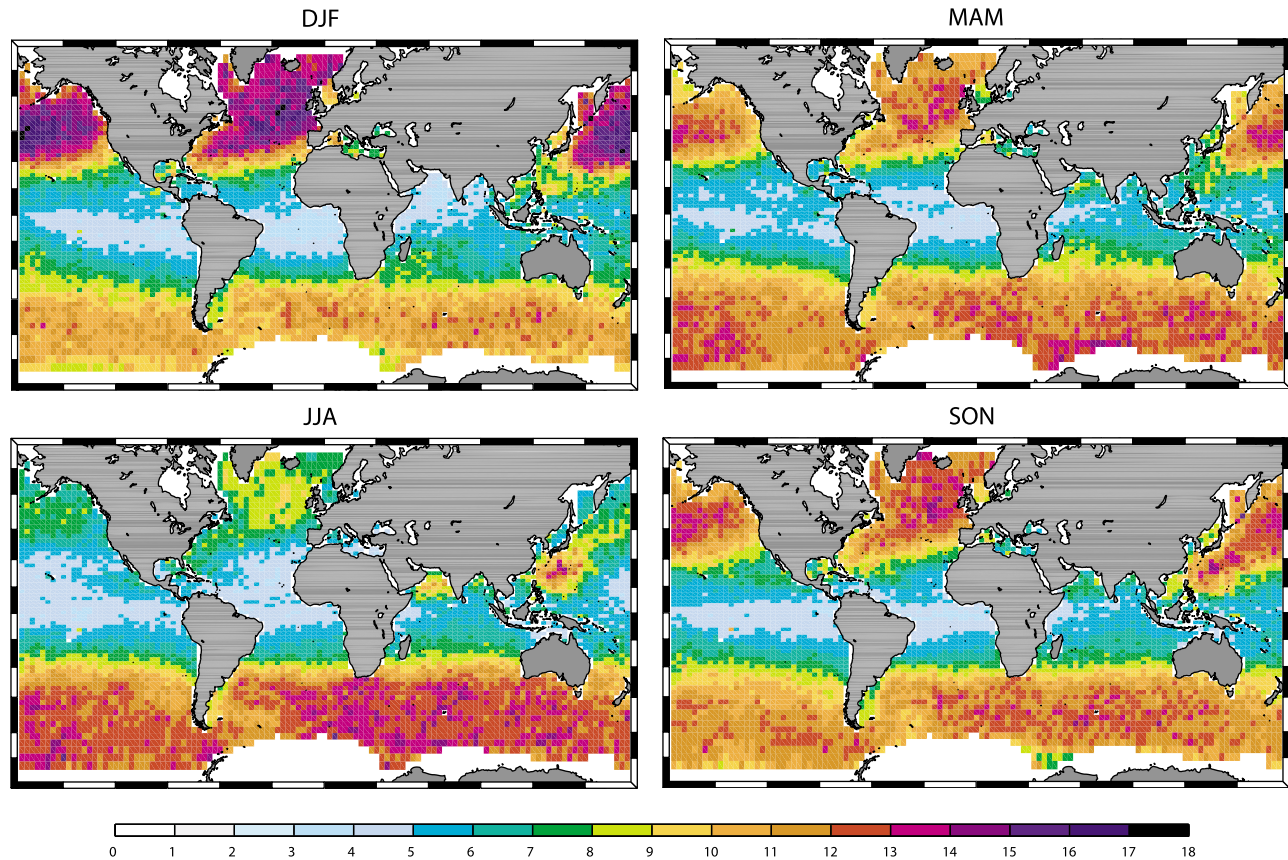


Figure 2. Seasonal distribution of the 20-year return level quantile, $H_{s_{20}}$ (m).

present a Fréchet like behavior: the Caribbean, the Gulf of Mexico, the western tropical Pacific (Philippine Sea) and French Polynesia. Areas of swell generation, such as the North Atlantic Ocean or the Austral Ocean (Roaring Forties) present Weibull distribution. This aspect of the behavior of the shape parameter is especially relevant when it comes to the estimation of high return-period quantiles, such as the 100 or 50 year return level values.

[11] Using the seasonal model we have obtained the quantile of extreme wave height for each season associated to a 20-year return level ($H_{s_{20}}$). Figure 2 shows the spatial distribution of the $H_{s_{20}}$ in December-January-February (DJF), March-April-May (MAM), June-July-August (JJA) and September-October-November (SON), which matches the spatial pattern obtained for $H_{s_{100}}$ by *Caires and Sterl* [2005] and *Alves and Young* [2003] and for $H_{s_{50}}$ by *Chen et al.*, [2004]. As expected, during the boreal winter (DJF) maximum values of $H_{s_{20}}$ are found in the North Atlantic and North Pacific Oceans. During the austral winter (JJA) the maximum $H_{s_{20}}$ are located in the Southern Ocean, concentrated between South Africa and Australia [Young, 1999] due to the extended fetch provided by the westerly winds. One can see that the seasonal variability of the extreme SWH in the Northern Hemisphere is much greater than in the Southern Hemisphere. A similar behavior was found for mean monthly values of SWH by *Young* [1999]. The most severe extreme wave climate in the North Pacific is registered south of the Aleutians in DJF ($H_{s_{20}} = 17.65$ m). In the North Atlantic Ocean, the highest values of $H_{s_{20}}$ are expected south of Iceland and southwest of Ireland (≈ 17 m), in the area of

winter storm generation. In the South Atlantic Ocean, during the austral winter $H_{s_{20}} \approx 15.5$ m is expected near the coast of South Africa. With regard to the Indian Ocean, higher values of $H_{s_{20}}$ during the austral winter near Indonesia and Madagascar are detected, due to swells coming from the storm generation area in the Southern Ocean. Note the increase of wave climate severity at the Arabian Sea during the Indian monsoon season (JJA) and in the South China Sea and Philippine Sea possibly due to the western north Pacific summer monsoon.

4.2. Interannual Variability

[12] Figure 3 summarizes in a mosaic the results for the climate-related patterns mentioned above. Two global climate indices characterize non-seasonal variations in both hemispheres. The AO index is the dominant pattern north of 20°N while the SAM index represents its counterpart south of 20°S (β_{AO} and β_{SAM} in Figures 3a and 3b respectively). According to Figure 3a, the AO index has a significant influence in the North Atlantic Ocean with a clear spatial pattern. Positive phases of the AO contribute to the extreme wave height in the Norwegian Sea and south of Iceland with a maximum of 70 cm/unit of AO, while negative phases contribute to the extreme wave height in the area south the Azores with lower intensity. Considering a specific instant (not shown), on February 2010, the AO index was -4.13 , which means that 2.06 m of extreme wave height in the Azores was explained by the influence of the AO index. Figure 3b shows a less intense but a widespread influence of the SAM index. Positive phases of the SAM increase extreme

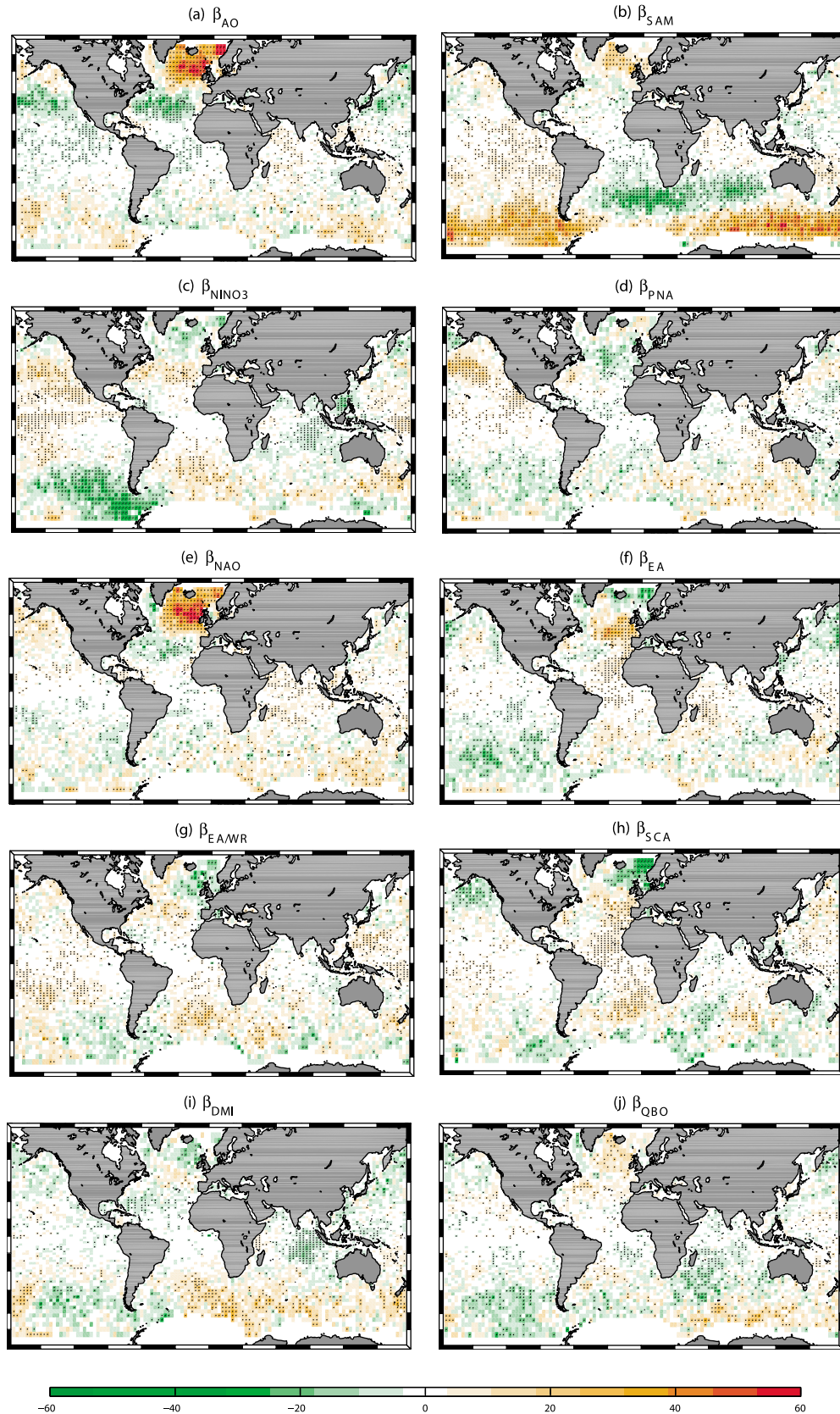


Figure 3. Spatial variability of the influence of the climate indices on the location parameter (cm/unit). Only statistically significant values at the 90% confidence interval are dotted. All figures are bounded to -60 and 60 cm.

wave heights along the Pacific and Indian part of the Southern Ocean (up to 60 cm/unit), consistent with the study of *Hemer et al.* [2010]. Negative phases contribute to extreme wave heights in the South Atlantic and South Indian Oceans (up to -60 cm/unit).

[13] The NINO3 index characterizes El Niño-Southern Oscillation phenomenon through the eastern tropical Pacific sea surface temperature [Rasmusson and Carpenter, 1982]. In Figure 3c, a clear pattern of influence of the NINO3 along the Pacific Ocean is found. During El Niño events, extreme wave heights suffer an increase along the equatorial latitude of the western-central Pacific Ocean, including the Tasman Sea, and the eastern North Pacific Ocean (up to 25 cm/°C). The highest Niño event registered in this period was in December 1997, when the NINO3 was 4.2 °C; therefore, 1.05 m of extreme wave height in the central Pacific, the Tasman Sea and the north east Pacific was due to the influence of the ENSO. On the other hand, during La Niña phase, extreme wave height in the southeastern Pacific is intensified, finding the most influence in the Drake Passage. A teleconnection in the North Atlantic (Azores area) for positive phases of NINO3 and in the mid Indian Ocean and the South China Sea during negative phases of NINO3 is also detected. One of the most prominent modes of low-frequency variability in the Northern Hemisphere extra tropics that affects the Pacific Ocean is the PNA [Wallace and Gutzler, 1981]. A positive pattern of PNA (Figure 3d) is located over the eastern-north Pacific. During positive phases of PNA, 45 cm/unit of extreme wave height southward of the Aleutians and 30 cm/unit of extreme wave height close to the coast of Baja California and Mexico are explained due to this climate index.

[14] In the North Atlantic, the NAO [Barnston and Livezey, 1987] and EA pattern have been chosen. Moreover, the EA/WR pattern affecting Eurasia [Barnston and Livezey, 1987] and the SCA that affects Scandinavia complete the climate patterns used. Figures 3e–3h show the spatial variability of the influence of the NAO, EA, EA/WR and SCA on the location parameter (β_{NAO} , β_{EA} , $\beta_{EA/WR}$, β_{SCA}), respectively. In Figure 3e, the NAO influence is found to be similar to the AO's but less spread out. This is due to the fact that the NAO pattern is the offshoot of the AO. Positive phases of NAO increase the extreme wave height south of Iceland and close to the east coasts of Ireland and Great Britain at a maximum of 75 cm/unit; in February 1997 the NAO index registered 5.2 units, with 3.9 m of extreme wave height being due to the influence of the NAO. The NAO index affects the extreme SWH along the Azores with less intensity and expansion than its northward dipole. The influence of NAO index in the northeast Atlantic can be associated to swell variations [Gulev and Grigorieva, 2006]. The influence of the EA pattern spans along the east Atlantic Ocean. Positive phases of the EA pattern affect the extreme wave height of mid and tropical latitudes of the eastern-north Atlantic Ocean, intensifying its influence on the Atlantic coast of southern Europe (40 cm/unit). Negative phases affect the extreme wave height of the Norwegian and Mediterranean Sea. Results for the EA/WR pattern reveal a slightly negative influence on the North Atlantic-Norwegian Sea and the Mediterranean. The regional nature of this climate index requires a higher resolution to extract better information about its influence on extreme wave climate [Izaguirre et al., 2010]. Finally, the spatial variability of the influence of the

SCA pattern shows a spatial pattern similar to the EA's but more widespread during positive phases. The negative phase of the SCA pattern contributes to an increase of the extreme wave height along the Norwegian, North and Baltic Sea (up to 65 cm/unit).

[15] Finally, two climate indices representative of the Indian Ocean have been chosen, the Indian Ocean Dipole (IOD) [Saji et al., 1999], measured by the DMI and the QBO, also known as Singapore Winds. Figures 3i and 3j show the spatial pattern of the influence of DMI and QBO indices. Positive phases of DMI increase the extreme wave height in the confluence of the south Atlantic with the Southern Ocean and in the south western Pacific, close to the coast of New Zealand. Negative phases of DMI contribute to increase the extreme wave height in the eastern Indian Ocean, close to the coasts of Indonesia and Sri Lanka (up to -50 cm/unit). Finally, the pattern of influence of QBO is detected during negative phases of the index, spreading over the south west of the Indian Ocean.

5. Conclusions

[16] The seasonal-to-interannual variability of the global extreme wave height is analyzed using satellite data by means of a time dependent generalized extreme value model. Seasonality has been modeled through harmonic functions that represent the annual cycle in the location and scale parameters. Interannual variability is explained via climate indices, which are included as covariates in the location parameter of the GEV distribution.

[17] Results of this work show that the most severe extreme wave climate around the globe is observed at higher latitudes. The effects of phenomena such as hurricanes, tropical cyclones or typhoons on extreme wave climate are detected by the Fréchet behavior shown by the shape parameter of the GEV distribution. Moreover, the interannual variability analysis reveals the AO, SAM and NINO3 indices as being the most influential climate patterns in extreme wave height around the world. The AO presents significant influence on the Atlantic Ocean with a dipole spanning between Iceland, the Norwegian Sea and the Azores. The SAM presents a widespread influence along the Southern Ocean and South Indian and South Atlantic Ocean. Finally, the NINO3 contributes to the extreme wave height along the western-central Pacific and the North Pacific in positive phases while negative phases increase the extreme wave height in the Drake Passage and the Indian Ocean. Other climate indices representative of the Atlantic, Pacific and Indian Ocean have been used to model interannual variability finding more regional results, such as the NAO for the North Atlantic, the PNA for the Eastern North Pacific and the DMI for the Indian Ocean. We believe that these findings can be useful to explain and predict extreme events in coastal areas.

[18] **Acknowledgments.** The work was partially funded by projects "GRACCIE" (CSD2007-00067, CONSOLIDER-INGENIO 2010) from the Spanish Ministry of Science and Technology, "MARUCA" (200800050084091) from the Spanish Ministry of Public Works and "C3E" (E17/08) from the Spanish Ministry of Environment, Rural and Marine Affairs.

[19] The Editor thanks two anonymous reviewers for their assistance in evaluating this paper.

References

- Alves, J. H. G. M., and I. R. Young (2003), On estimating extreme wave heights using 297 combined Geosat, Topex/Poseidon and ERS-1 altimeter data, *Appl. Ocean Res.*, *25*, 167–186, doi:10.1016/j.apor.2004.01.002.
- Barnston, A. G., and R. E. Livezey (1987), Classification, seasonality and persistence of low-frequency atmospheric circulation patterns, *Mon. Weather Rev.*, *115*, 1083–1126, doi:10.1175/1520-0493(1987)115<1083:CSAPOL>2.0.CO;2.
- Caires, S., and A. Sterl (2005), 100-year return value estimates for ocean wind speed and significant wave height from the ERA-40 data, *J. Clim.*, *18*, 1032–1048, doi:10.1175/JCLI-3312.1.
- Chen, G., S. W. Bi, and R. Ezraty (2004), Global structure of extreme wind and wave climate derived from TOPEX altimeter data, *Int. J. Remote Sens.*, *25*(5), 1005–1018, doi:10.1080/01431160310001598980.
- Cotton, P. D. (1998), A feasibility study for a global satellite buoy inter-calibration experiment, *Resolut. Consult. Rep. 26*, Southampton Oceanogr. Cent., Southampton, U. K.
- Gulev, S. K., and V. Grigorieva (2004), Last century changes in ocean wind wave height from global visual wave data, *Geophys. Res. Lett.*, *31*, L24302, doi:10.1029/2004GL021040.
- Gulev, S. K., and V. Grigorieva (2006), Variability of the winter wind waves and swell in the North Atlantic and North Pacific as revealed by the voluntary observing ship data, *J. Clim.*, *19*, 5667–5685, doi:10.1175/JCLI3936.1.
- Hemer, M. A., J. A. Church, and J. R. Hunter (2010), Variability and trends in the directional wave climate of the Southern Hemisphere, *Int. J. Climatol.*, *30*, 475–491.
- Hogben, N. (1995), Increases in wave heights over the North Atlantic: A review of the evidence and some implications for the naval architect, *Trans. R. Inst. Nav. Archit.*, *137*, 93–115.
- Izaguirre, C., F. J. Méndez, M. Menéndez, A. Luceño, and I. J. Losada (2010), Extreme wave climate variability in southern Europe using satellite data, *J. Geophys. Res.*, *115*, C04009, doi:10.1029/2009JC005802.
- Lionello, P., and A. Sanna (2005), Mediterranean wave climate variability and its link with NAO and Indian monsoon, *Clim. Dyn.*, *25*, 611–623, doi:10.1007/s00382-005-0025-4.
- Méndez, F. J., M. Menéndez, A. Luceño, and I. J. Losada (2007), Analyzing monthly extreme sea levels with a time-dependent GEV model, *J. Atmos. Oceanic Technol.*, *24*, 894–911, doi:10.1175/JTECH2009.1.
- Menéndez, M., F. J. Méndez, I. J. Losada, and N. E. Graham (2008), Variability of extreme wave heights in the northeast Pacific Ocean based on buoy measurements, *Geophys. Res. Lett.*, *35*, L22607, doi:10.1029/2008GL035394.
- Menéndez, M., F. J. Méndez, C. Izaguirre, A. Luceño, and I. J. Losada (2009), The influence of seasonality on estimating return values of significant wave height, *Coastal Eng.*, *56*(3), 211–219, doi:10.1016/j.coastaleng.2008.07.004.
- Rasmusson, E. M., and T. H. Carpenter (1982), Variations in tropical sea surface temperature and surface wind fields associated with the Southern Oscillation/El Niño, *Mon. Weather Rev.*, *110*, 354–384, doi:10.1175/1520-0493(1982)110<0354:VITSST>2.0.CO;2.
- Saji, N. H., B. N. Goswami, P. N. Vinayachandran, and T. Yamagata (1999), A dipole mode in the tropical Indian Ocean, *Nature*, *401*, 360–363, doi:10.1038/43854.
- Wallace, J. M., and D. S. Gutzler (1981), Teleconnections in the geopotential height field during the Northern Hemisphere winter, *Mon. Weather Rev.*, *109*, 784–812, doi:10.1175/1520-0493(1981)109<0784:TITGHF>2.0.CO;2.
- Wang, X. L., and V. R. Swail (2001), Changes of extreme wave heights in Northern Hemisphere oceans and related atmospheric circulation regimes, *J. Clim.*, *14*, 2204–2221, doi:10.1175/1520-0442(2001)014<2204:COEWHI>2.0.CO;2.
- Woolf, D. K., and P. G. Challenor (2002), Variability and predictability of the North Atlantic wave climate, *J. Geophys. Res.*, *107*(C10), 3145, doi:10.1029/2001JC001124.
- Young, I. R. (1999), Seasonal variability of the global ocean wind and wave climate, *Int. J. Climatol.*, *19*, 931–950, doi:10.1002/(SICI)1097-0088(199907)19:9<931::AID-JOC412>3.0.CO;2-O.

C. Izaguirre, I. J. Losada, F. J. Méndez, and M. Menéndez, Environmental Hydraulics Institute, Universidad de Cantabria, E.T.S.I. Caminos Canales y Puertos Avda. de los Castros s/n, E-39005 Santander, Spain. (mendezf@unican.es)